JOURNAL OF MATERIALS SCIENCE 35 (2000) 4977–4987

Thermal analysis of copper-tin alloys during rapid solidification

J. MAHMOUDI, H. FREDRIKSSON
Department of Materials Processing, Royal Institute of Technology, Stockholm, Sweden
E-mail: hasssef@matpr.kth.se

A series of solidification experiments using a mirror furnace and a levitation technique were performed on different Cu-Sn alloys. Cooling curves during solidification were registered using a thermocouple of type "K" connected to a data acquisition system. The undercooling, cooling rates of the liquid and of the solid state, solidification times and temperatures were evaluated from the curves. The samples were found to solidify far below the liquidus temperature. The cooling curves for different samples and alloys were simulated using a "FEM" solidification program. The heat transfer coefficient, heat of fusion and specific heat were evaluated. It was found that the calculated values of the heat of fusion were much lower than the tabulated ones. The calculated values of the specific heat in the solid state were also found to be much higher than those quoted in the literature, especially for the mirror furnace experiments. The effect of rapid cooling on the thermodynamic state and the solidification process of the alloys has been evaluated. The effect of cooling rate on the formation and condensation of vacancies is discussed. It is proposed that a large number of vacancies form during rapid solidification and that they condense during and after the solidification. The influence of these defects on the thermodynamics and solidification of the alloys has been evaluated.

1. Introduction

The structure and properties of solidified alloys have been observed to be influenced by the cooling rate during solidification. Rapid solidification is known to result in the formation of metastable microstructures characterised by: 1) a supersaturation of defects (i.e., refinement of the grain size in micro-and nano-crystalline material, a high density of vacancies, or a lack of order), 2) an increase in the solid solubility above the equilibrium limit, 3) the formation of metastable crystalline, quasicrystalline or glassy phases [1–7].

It has also been shown that a large undercooling occurs during the solidification process when the cooling rate of the liquid phase is very high [8]. The correlation between the cooling rate and other thermodynamic quantities in connection with lattice defects, has been previously discussed [9–12].

A supersaturation of vacancies forms in a metal by quenching, mechanical deformation or energetic particle irradiation. The energies for the formation of vacancies have been studied before [13–15]. These vacancies can migrate and coalesce to form microscopic clusters at temperatures where the vacancy are mobile, generally $T \geq 0.3T_m$, where T_m is the melting temperature [4, 16–17].

It has also been proposed [9, 10] that during solidification, a large number of vacancies forms in the metal lattice. The concentration of vacancies depends on the cooling conditions. When the alloy is rapidly quenched from a high temperature, there will be insufficient time for the new equilibrium concentration to be established and a large number of vacancies will be trapped. The increase in the concentration of vacancies will have an influence on the solidification process. The results have been discussed in connection with the formation of lattice defects [18, 19]. There is also a tendency for vacancies to be attracted to each other and form divacancies and finally clusters [20]. Some clusters collapse into dislocation loops, which can grow by absorbing more vacancies. Apart dislocations, the main sinks for excess vacancies are the grain boundaries and other interfaces within the specimens.

The purpose of this work is to analyse the formation and condensation of vacancies during solidification. The effect of the vacancies on the thermodynamic parameters during the solidification of Cu-Sn alloys are also investigated theoretically.

2. Materials and methods

A number of experiments using different cooling rates were performed with pure copper and copper-tin alloys containing 2, 4, 6, 11% Sn. All the alloys were produced from highly pure elements using a vacuum induction or arc-melting furnace under argon atmosphere. Different types of solidification experiments at different cooling rates were performed using the following techniques:

2.1. Levitation equipment

Higher cooling rates, up to 110,000 $^{\circ}\mathrm{K\,s^{-1}}$, were achieved by using a levitation technique. Briefly a sample weighing 1–1.5 g was levitated and melted without a crucible in an induction furnace, and cast in a rectangular copper mould. An open thermocouple of type "*K*" with a diameter of 0.1 mm was inserted in to the base of the mould, to record temperature. The set of the mould with thermocouple was inserted to the glass levitation tube. The experiments were performed under an argon atmosphere. The thermocouple was connected to a data acquisition system that allowed the collection of data with an interval of 0.15 milliseconds; the data were plotted as a cooling curve. The process is described in details elsewhere [21]. Typical cooling curves obtained from levitation experiments are plotted in Fig. 1a.

2.2. Mirror furnace

Mirror furnace was used to achieve cooling rates between 20 and 120 $\mathrm{K\,s^{-1}}$. A cylindrical sample ($D = 3$ mm, $L = 6.5$ mm) was placed inside an evacuated quartz tube. A hole ($D = 1.25$ mm, $L = 3.25$ mm) was drilled in the sample for inserting thermocouple of type "*K*". The quartz tube containing the sample was placed in the mirror furnace, which consisted of two high power lamps placed between two ellipsoidal mirrors with the sample in the common point of focus.

The sample was firstly preheated to 700–900 °C, and then superheated to 60–80°C, and maintained at that temperature for a few seconds to achieve thermal equilibrium. It was then cooled in an air/gas stream. Cooling curves were obtained using suitable recording equipment.

A more complete description of the experimental technique can be found elsewhere [22]. Typical cooling curves obtained from mirror furnace experiments are plotted in Fig. 1b.

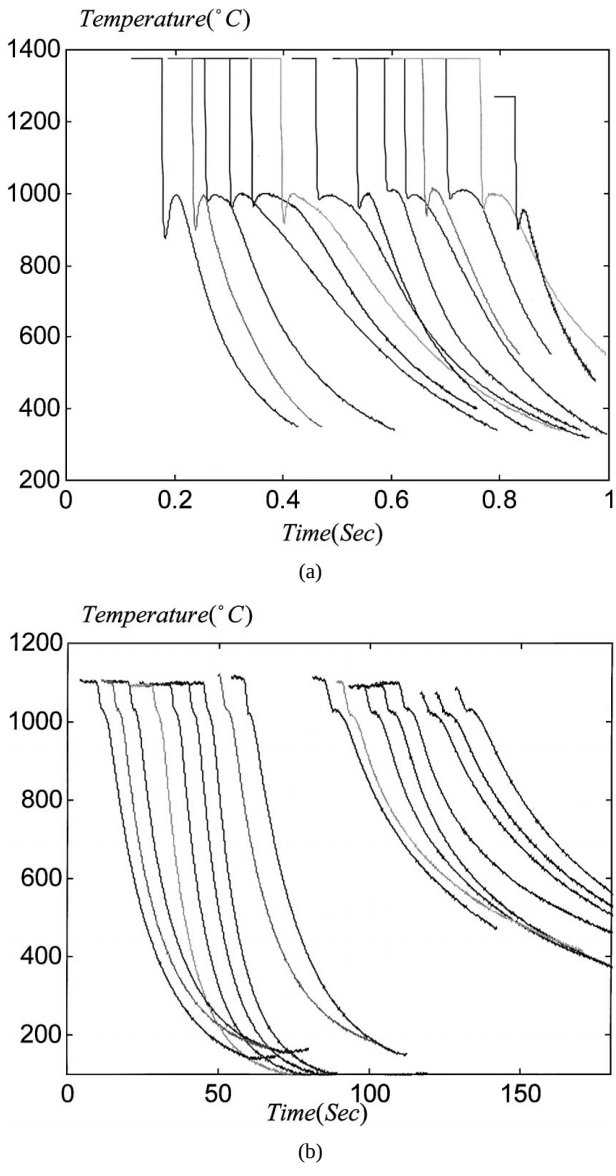

Figure 1 Typical cooling curves for different Cu-4% Sn alloys in a) levitation and b) mirror furnace experiments.

3. Thermal analysis for estimation of thermodynamic properties

In earlier work [19], the authors made a one dimensional heat evaluation for a sample during solidification:

$$\frac{\mathrm{d}Q}{\mathrm{d}t} = V\rho\left(C_{\mathrm{p}}\frac{\mathrm{d}T_{\mathrm{S}}}{\mathrm{d}t} + \Delta H\frac{\mathrm{d}\,f_{\mathrm{s}}}{\mathrm{d}t}\right) \tag{1}$$

Where $\mathrm{d}T_{\mathrm{S}}/\mathrm{d}t$ is the cooling rate of the sample and $\mathrm{d}\,f_{\mathrm{s}}/\mathrm{d}t$ is the transformation rate during solidification.

In this work, the solidification process is calculated by solving Fourier's heat equation in two dimensions. The principal features are outlined below.

$$\rho C_{\mathrm{p}}\frac{\mathrm{d}T}{\mathrm{d}t} = \mathrm{div}(k\,\mathrm{grad}T) + \dot{q} \tag{2}$$

Here ρ is material density, C_{p}, is specific heat, T is temperature, k is heat conductivity and $\mathrm{d}T/\mathrm{d}t$ is the cooling rate of the sample. The source term, $\dot{q}$, is described as:

$$\dot{q} = \begin{cases} 0 & \text{when} \quad T > T_{\mathrm{L}} \\ \rho\Delta H\frac{\mathrm{d}\,f}{\mathrm{d}t} & \text{when} \quad T_{\mathrm{S}} < T < T_{\mathrm{L}} \\ 0 & \text{when} \quad T < T_{\mathrm{S}} \end{cases} \tag{3}$$

Where ΔH is the latent heat release during solidification, and the fraction of the solid phase, f_{s}, varies from 0 to 1. The transformation rate during solidification, $\mathrm{d}\,f/\mathrm{d}t$ is described by the solidification rate, g, as follow:

$$\frac{\mathrm{d}\,f}{\mathrm{d}t} = g(T,\ f)$$

The model is supplemented by suitable boundary conditions, expressing heat flow by radiation and heat exchange. Heat extraction from the sample to the surroundings can be obtained from the following relation:

$$-k\left(\frac{\partial T}{\partial n}\right) = h(T_{\mathrm{S}} - T_0) + \sigma\varepsilon\left(T_{\mathrm{S}}^4 - T_0^4\right) \tag{4}$$

where $\partial T/\partial n$ is the outward normal derivative, σ is the Boltzmann constant, ε is the emissivity of the radiating

surface, T_0 is the ambient temperature, h is heat transfer coefficient and T_S is the temperature of the sample.

The accurate modelling of this process requires a validated description of the boundary conditions. It was assumed that heat is lost from the sample to the surroundings at a rate controlled by the heat transfer coefficient. The greater the value of h, the larger is the heat flow out from the sample. In this work, it was assumed that a constant heat transfer coefficient exists at the interface of the sample and the mould/glass tube for the levitation/mirror furnace experiments. Note that, for mirror furnace experiments, the heat conductivity in metal is very high compared to the heat conductivity in the glass tube. This results in a very small temperature gradient in the sample. For the levitation experiments, heat flow is controlled by resistance at the mould-metal interface and most temperature drop occurs at the interface.

Moreover,

$$T(x, y, 0) = T_{\max} \quad \text{at} \quad t = 0,$$

where $T_{\max}$ is the initial temperature at the starting point of the cooling process. It is in general impossible to find an analytical solution to this problem. Solutions must be obtained by numerical methods and the calculations presented here are based on the Finite-Element-Method (FEM), using a program called CASTFEM [23].

3.1. Numerical treatment

The partial differential Equations 2–4 of heat transport with phase change in two dimensions can be combined and solved with a finite element method.

The FEM base program, CASTFEM, which has been modified to describe the case studied here, was used to evaluate heat transfer from the sample to its surroundings. The pre and post-processor for the program, FEMGV4 [24] was used to generate the mesh. Equation 2 is discretized by conventional finite elements, three nodes triangles in two-dimensional models of the material in the sample and in the mould/glass tube for the levitation/mirror furnace experiments. A mesh consisting of four-nodded elements, was used to define the gap between the sample and mould or glass tube.

Due to the symmetry of the samples for the mirror-furnace and the levitation experiments, only one quarter of the specimens needed to be modelled. Suitable time steps and element sizes were determined by a series of preliminary computations for each case. Typical FEM models used for the numerical analyses, for the levitation technique and for the mirror furnace equipment, are shown in Fig. 2a and b.

Appropriate relationships, which describe the initial temperature conditions of the different materials, in the sample and in the mould/glass tube for the levitation technique/mirror furnace equipment, have been considered. The boundary conditions including the heat transfer coefficient, h, as a constant value during the solidification process, the emissitivity factor, ε, and the boundary temperature were added. Material data for the sample and mould or glass tube (for each case) included heat conductivity, k, the evaluated value for the specific heat for the solid, the latent heat of fusion, the liquidus and the solidus temperatures were also considered.

TABLE I Tabulated physical data used for numerical computation

Alloy	T_l (K)	ΔH (J Kg^{-1})	C_P (J kg K^{-1})	ρ (K gm^{-3})
Cu	1356	205e3	495	8000
Cu-2%Sn	1352	235e3	520	7980
Cu-4%Sn	1335	270e3	530	7960
Cu-6%sn	1328	295e3	530	7940
Cu-11%Sn	1283	340e3	490	7890

TABLE II Other operating parameter used for computation

Parameter	Value
D (m s^{-2})	4e-11
λ (m)	1e-6-7e-6
σ (W m^{-2} K^{-4})	5.669e-8
ε	0.04–0.57
$C_{p,\,mould}$ (J kg K^{-1})	385
K_{mould} (W m^{-1} K^{-1})	401
ρ_{mould} (K g m^{-3})	8900
$C_{p,\,glass\,tube}$ (J kg K^{-1})	820
$k_{glass\,tube}$ (W m^{-1} K^{-1})	182
$\rho_{glass\,tube}$ (K g m^{-3})	2100

The thermophysical data of the mould and the metal, presented in Tables I and II, were obtained from the literature [25–29] or well-known Thermo-calc program [30], and carefully adapted to the experimental conditions for each case. In order to find the proper range of values for different operating condition such as emissivity of the radiating surface and heat transfer coefficient, a series of numerical computations with different ε and h was carried out. It was found that the contribution of variation of ε is negligible. The heat transfer coefficient was determined by fitting the data prior to the solidification. The latent heat was varied during the solidification process to find proper agreement between the simulated and experimented cooling curves.

3.2. Simulation of solidification

Fig. 3a and b shows typical simulated cooling curves for both the levitation technique and the mirror furnace experiments at the centre of the sample, where the thermocouple is normally inserted. The measured cooling curves from the experiments are also shown in Fig. 3 for each case.

4. Results

Typical cooling curves obtained from the levitation techniques and from the mirror furnace experiments on the Cu-4%Sn alloy were earlier shown in Fig. 1a and b. The cooling curves often show a fairly large undercooling followed by a recaleascence. Some experiments did not show any recalescence, but instead contained a plateau temperature. The maximum recalesence or the plateau temperature was chosen as the solidification temperature. Start and end of solidification were chosen as the point where the slope of the temperature-time

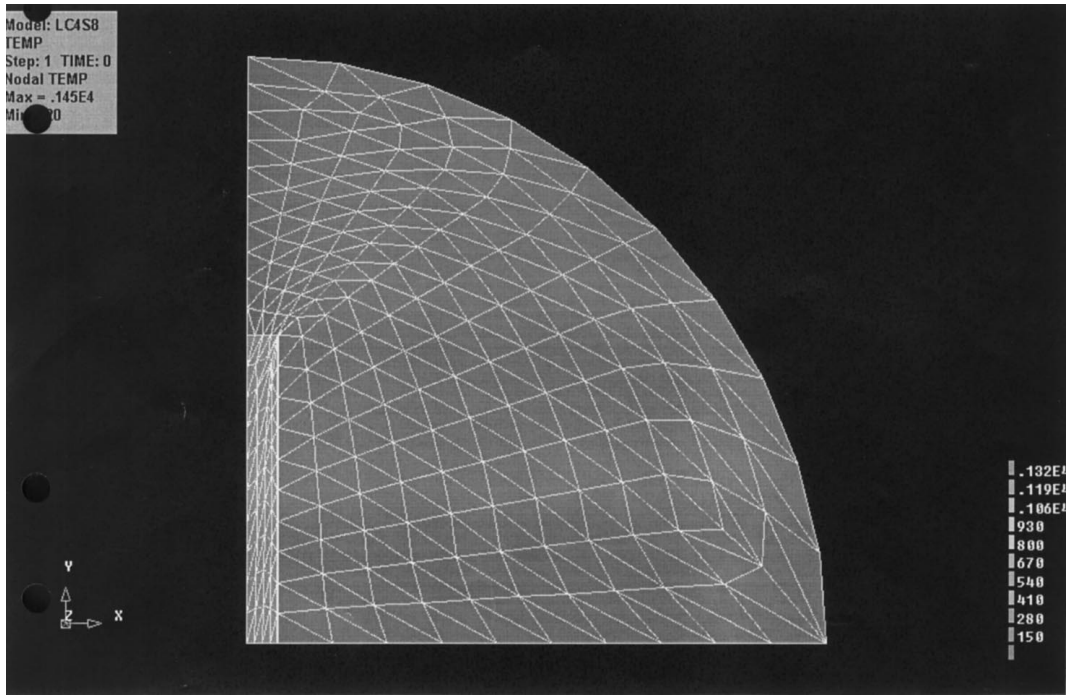

(a)

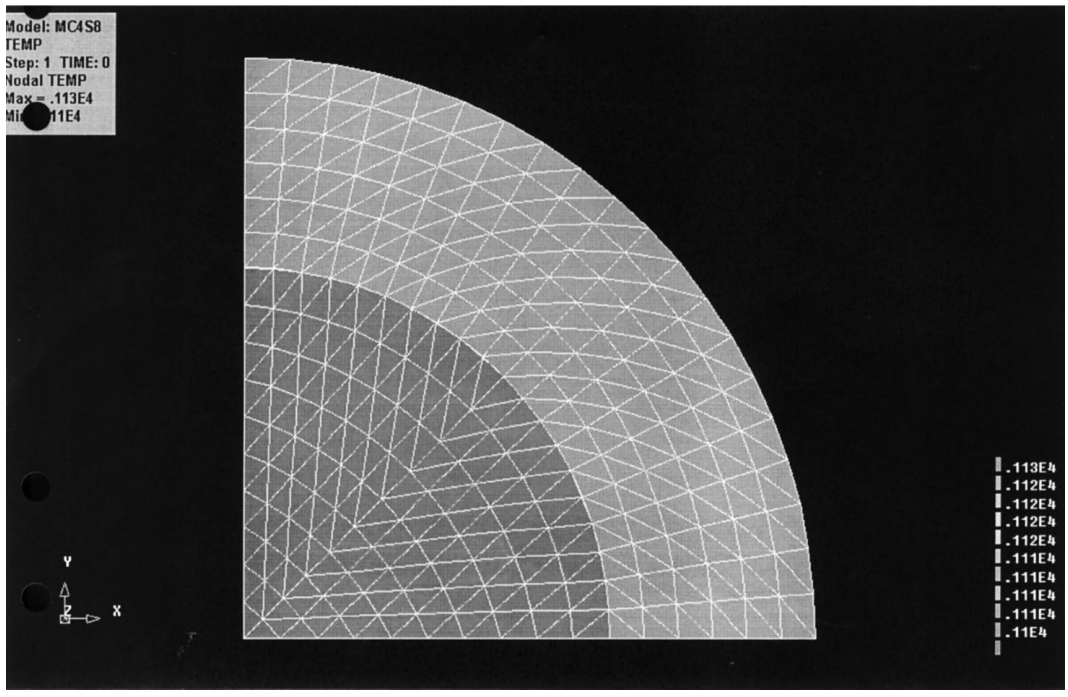

(b)

Figure 2 Two-dimensional FEM model for a) levitation and b) mirror furnace experiments.

curve of the sample was changed. However, it was often difficult to determine the time for the end of the solidification.

The cooling rates in the liquid and solid state, the solidification temperature, T_m, the solidification time and the undercooling temperature were evaluated from the curves.

4.1. Solidification undercooling

Fig. 4a and b shows the relationship between the solidification undercooling and the cooling rate in liquid for Cu and different Cu-Sn alloys. The cooling rate was varied between 20 K s^{-1} in the mirror furnace experiments, to a maximum of 110,000 K s^{-1}, in the levitation experiments. It can be seen that the solidification temperature decreases, and consequently, the undercooling increases by increasing the cooling rate in the liquid.

The undercooling normally reaches the highest value for each case at the highest cooling rate. The results will be discussed later in connection with the formation of lattice defects.

4.2. Heat of fusion

Fig. 5a and b shows the calculated fraction of latent heat, $\Delta H_{meas}/H_{tab}$, versus cooling rate for the different alloys. The results show that the calculated values for

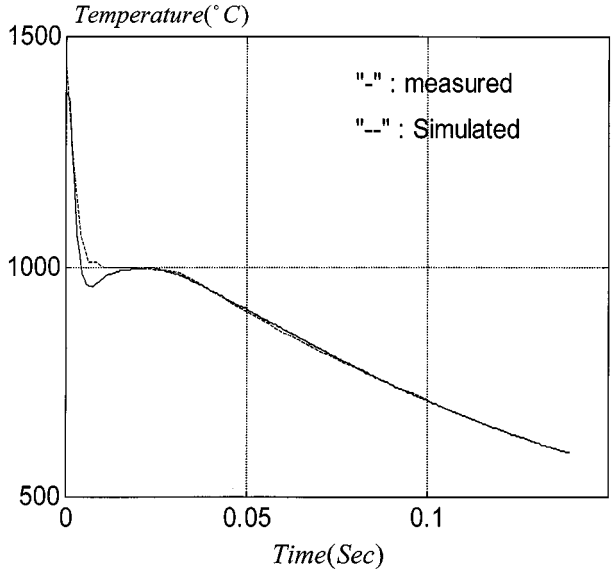

(a)

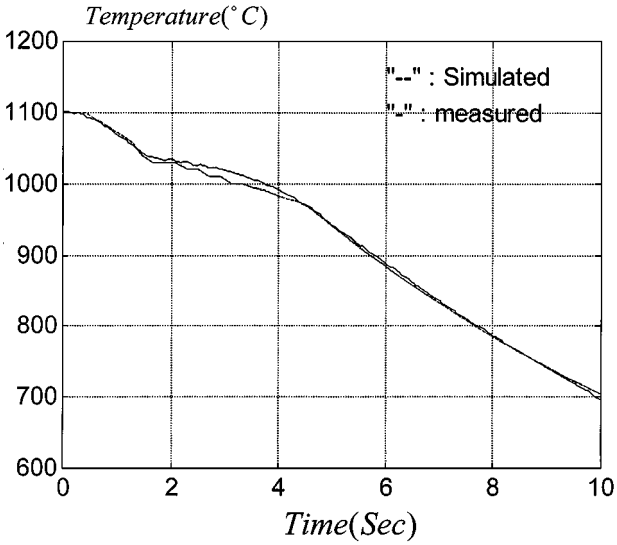

(b)

Figure 3 Typical simulated and measured cooling curves for Cu-4% Sn during a) levitation and b) mirror furnace experiments.

heat of fusion are much lower than the tabulated ones. The figure also shows that an increase in cooling rate will decrease the values for ΔH.

This relation can generally be described by:

$$\Delta H = f\left(\frac{\mathrm{d}T}{\mathrm{d}t}\right)$$

A satisfying agreement was found when the results were compared with what has been presented and discussed earlier [19].

4.3. Specific heat capacity

Fig. 6a and b shows the variation in specific heat versus cooling rate for the solid state. It is interesting to note that the specific heat for a solid phase is much higher than the values found in literature; this is especially the case in the mirror furnace experiments. At higher cooling rates it decreases down to the tabulated value. The results will later be discussed in connection with the condensation of vacancies after solidification process.

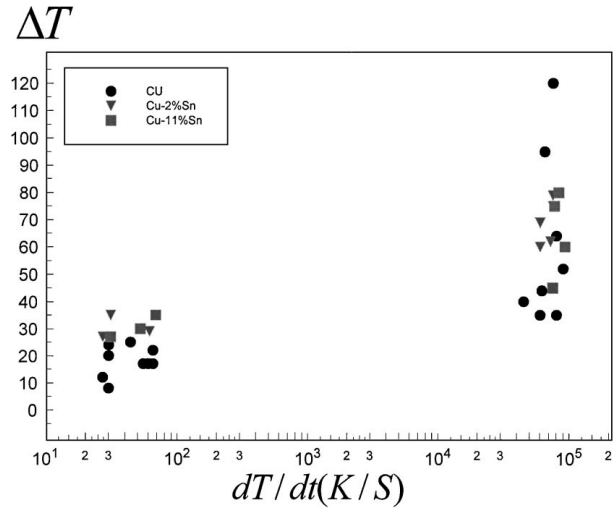

(a)

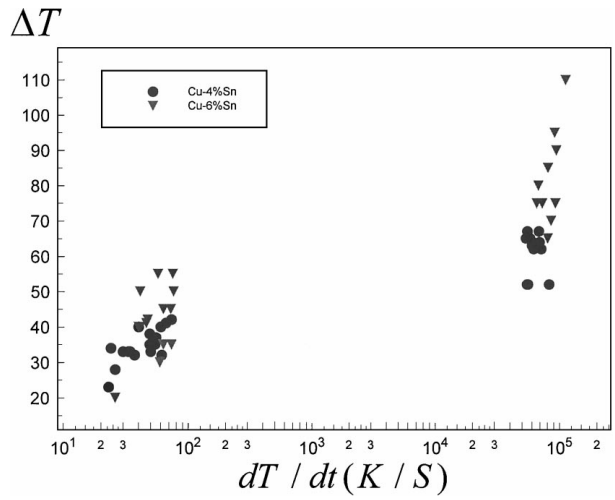

(b)

Figure 4 Solidification undercooling temperature vs. the cooling rate in liquid for a) Cu, Cu-2%Sn, Cu-11%Sn and b) Cu-4%Sn, Cu-6% Sn.

5. Discussion

In an earlier work [19] and [9, 18], it was stated that during solidification, a large number of lattice defects such as vacancies form and then condense. The concentration of vacancies that form in the lattice depends on the cooling conditions. When the alloy is rapidly quenched from the melting temperature, there is insufficient time to reach an equilibrium concentration of vacancies. A high concentration of vacancies will thus be trapped in the solid. The formation of lattice defects will change the thermodynamic properties of the metals.

The difference in density between the solid and liquid can be assumed to cause the majority of the vacancies formed:

$$y_v \propto \frac{\Delta\rho}{\rho_{\mathrm{s}}^{\mathrm{eq}}} \quad \text{and} \quad \Delta\rho_{\mathrm{V}} \leq \rho_{\mathrm{s}}^{\mathrm{eq}} - \rho_{\mathrm{l}}^{\mathrm{eq}},$$

where $\rho_{\mathrm{s}}^{\mathrm{eq}}$ = equilibrium density of solid; $\rho_{\mathrm{l}}^{\mathrm{eq}}$ = equilibrium density of liquid.

It is thus expected that the maximum fraction of vacancies in copper is around 0.06–0.08 which is roughly 100 times the equilibrium value [9]. It is worth noting that the fraction of vacancies formed in the solid varies with the cooling rate.

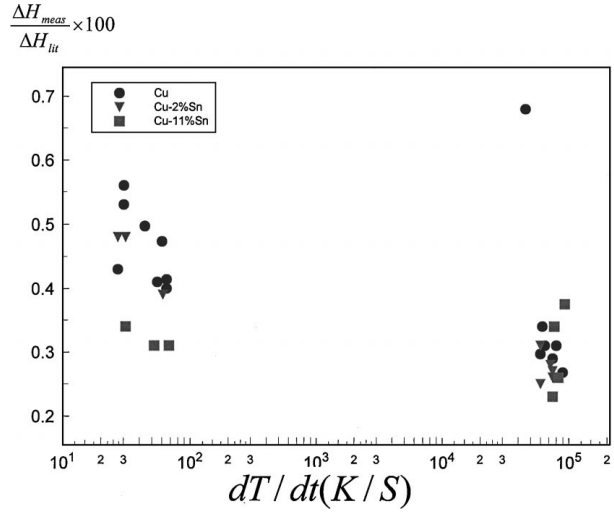

(a)

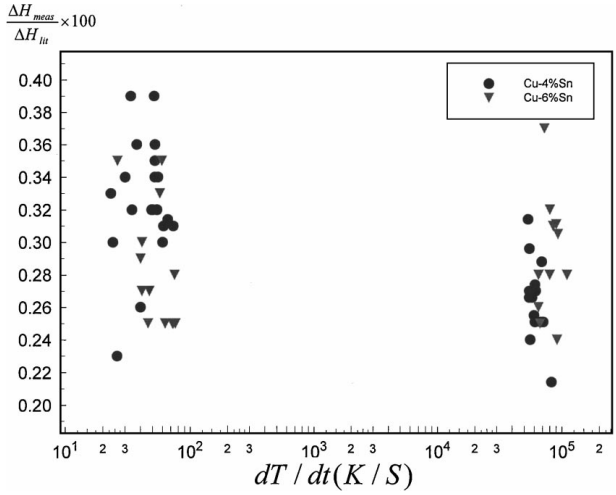

(b)

Figure 5 Heat of fusion vs. cooling rate in liquid for a) Cu, Cu-2%Sn, Cu-11%Sn and b) Cu-4%Sn, Cu-6% Sn.

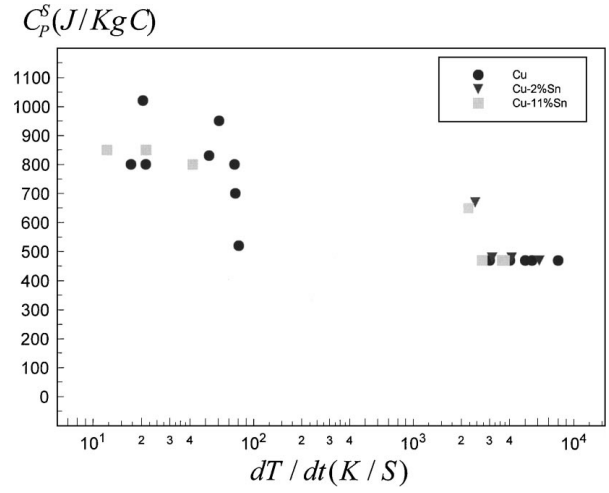

(a)

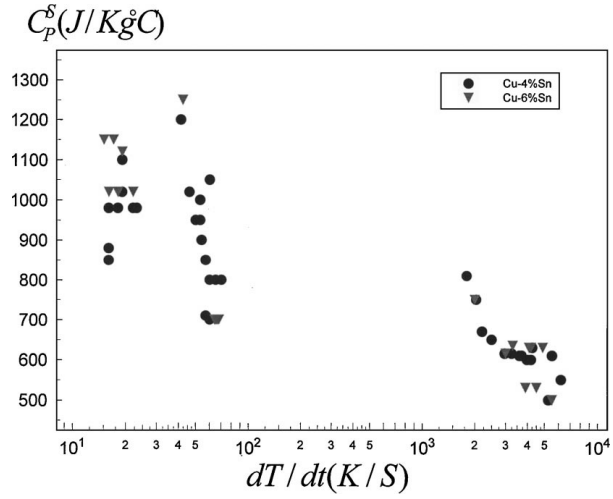

(b)

Figure 6 Specific heat vs. cooling rate in the solid zone for a) Cu, Cu-2%Sn, Cu-11%Sn and b) Cu-4%Sn, Cu-6% Sn.

The change in Gibbs free energy during the formation of vacancies is denoted by:

$$G_{\mathrm{v}} = H_{\mathrm{v}} - TS_{\mathrm{v}}. \tag{5}$$

This change consists of an enthalpy contribution, H_{v}, and an entropy contribution TS_{v}. If N_{v} vacancies are created at a lattice site, N, the configurational entropy is given by Boltzmann's statistical interpretation of the entropy as:

$$S_{n\mathrm{v}} = k \ln \frac{(N + N_{\mathrm{v}})!}{N!}, \tag{6}$$

and the atomic concentration at a mono-vacant site can be introduced as:

$$y_{1\mathrm{v}} = \frac{N_{1\mathrm{v}}}{N}.$$

The equilibrium concentration of mono-vacancies can be found by looking for the minimum of $\Delta G_{1\mathrm{v}}$. The fraction of vacancies is very small and therefore, terms of the order $N_{1\mathrm{v}}/N$ can be neglected compared to unity.

$$y_{1\mathrm{v}}^{\mathrm{eq}} = \exp\left(\frac{\Delta S_{1\mathrm{v}}}{R}\right) \exp\left(-\frac{\Delta H_{1\mathrm{v}}}{RT}\right). \tag{7}$$

It has been mentioned [31] that vacancies form the highest equilibrium concentration of different defects in metals; at the melting temperature the equilibrium concentration is between 10^{-3} and 10^{-4}. The experiments and theoretical estimates [31] indicate that for metals, $S_{1\mathrm{v}}$, is in the same order of magnitude as Boltzmann's constant k, when a typical order of magnitude for $H_{1\mathrm{v}}$ is $10kT_{\mathrm{m}}$, hence

$$T_{\mathrm{m}} S_{1\mathrm{v}} \ll H_{1\mathrm{v}},$$

It is necessary to distinguish between the total concentration of vacant sites, y_{v} and the concentration of mono-vacancies, $y_{1\mathrm{v}}$, or divacancies, $y_{2\mathrm{v}}$, etc. The total concentration of vacancies is given by:

$$y_{\mathrm{v}} = \sum_m m y_{m\mathrm{v}}.$$

In the present work, it is assumed that it is sufficient to consider mono-vacancies and divacancies.

In order to explain the effect of the formation and condensation of vacancies on the behaviour of solidification, the analysis will firstly be made of the thermodynamics of vacancies.

5.1. Thermodynamics of Cu-Sn-V

In this paper, vacancies, together with copper will be treated as a binary alloy system, and with copper and tin as a ternary alloy system. The binary Cu-V system has been discussed earlier [9, 19]. In this work a ternary Cu-Sn-V system is considered. The free energy for this system can be written as:

$$G_{\mathrm{m}} = y^0_{\mathrm{Cu}} G^0_{\mathrm{Cu}} + y^0_{\mathrm{Sn}} G^0_{\mathrm{Sn}} + y_{\mathrm{v}} G_{\mathrm{v}} + RT(y_{\mathrm{cu}} \ln y_{\mathrm{Cu}} + y_{\mathrm{Sn}} \ln y_{\mathrm{Sn}} + y_{\mathrm{v}} \ln y_{\mathrm{v}} + (1 - y_{\mathrm{v}}) \ln(1 - y_{\mathrm{v}})) + G^{\mathrm{EX}} \quad (8)$$

where y_{v} is the fraction of vacancies in one mole of the alloy. The following definition for the fraction of vacancies is used:

$$y_{\mathrm{v}} = \frac{N_{\mathrm{v}}}{N_{\mathrm{cu}} + N_{\mathrm{Sn}}}, \quad \text{when} \quad N_{\mathrm{Cu}} + N_{\mathrm{Sn}} = N$$

In this equation, N, N_{v}, N_{Cu} and N_{Sn} describe the number of lattice sites, vacant lattice sites, copper and tin lattice sites, respectively.

The excess Gibbs free energy, G^{Ex}, represents the deviation from ideal behaviour. For a binary Cu-Sn system G^{Ex} can be defined as:

$$G^{\mathrm{Ex}} = y_{\mathrm{Cu}} y_{\mathrm{Sn}} L_{\mathrm{cuSn}} \quad (9)$$

In this equation, L_{CuSn} is used to describe the interaction between Cu and Sn. The interaction between point defects in metals has been discussed earlier by March [32] and more recently by Fredriksson [20]. When L_{CuSn} is constant and independent of composition and temperature, one can talks about a *regular solution*.

For a solution with more than two components such as Cu-Sn-V, the interactions within each combination of two components should be considered. Bearing this in mind, G^{Ex} for a ternary Cu-Sn-V can be defined as:

$$G^{\mathrm{Ex}} = y_{\mathrm{Cu}} y_{\mathrm{Sn}} L_{\mathrm{cuSn}} + y_{\mathrm{Cu}} y_{\mathrm{v}} L_{\mathrm{CuV}} + y_{\mathrm{Sn}} y_{\mathrm{v}} L_{\mathrm{SnV}} + y_{\mathrm{v}} y_{\mathrm{v}} \Delta H_{2\mathrm{v}} \quad (10)$$

There is little information regarding the interaction between alloying elements and the vacancies for copper-base alloy. However, as was discussed by Fredriksson and Emi [20] L_{SnV} describes the tendency for the vacancies to form clusters of V and Sn, and $\Delta H_{2\mathrm{v}}$ describes their tendency to form *divacancies*. It was further, assumed that the interaction between vacancies and the solvent element is the same as the interaction between the solute element and vacancies. In this work, it is assumed that $\Delta H_{2\mathrm{v}}$ is independent of temperature, but increases by formation and trapping extra vacancies. In view of this, Equation 10 is modified to:

$$G^{\mathrm{Ex}} = y_{\mathrm{Cu}} y_{\mathrm{Sn}} L_{\mathrm{CuSn}} + y_{\mathrm{Sn}} y_{\mathrm{v}} L_{\mathrm{SnV}} + y_{\mathrm{v}} y_{\mathrm{v}} A \Delta H_{2\mathrm{v}} \quad (11)$$

TABLE III Thermodynamic data for vacancies and tin in pure copper

Parameter	Value
ΔH_{v} (J/m)	112.8e3
ΔS_{v} (J/mK)	12.4
$E_{2\mathrm{v}}$ (eV)	0.10–0.33
L_{CuSn} (eV)	0.22
$y^{\mathrm{eq}}_{\mathrm{v}}$	10^{-3}–10^{-4}

The constant, A, will be discussed in the next section. The interaction between Cu and Sn, L_{CuSn}, is given in Table III. The interaction between vacancies and tin, L_{SnV}, can be estimated using the equilibrium fraction of vacancies.

The equilibrium number of vacant sites $y^{\mathrm{eq}}_{\mathrm{v}}$, for a Cu-Sn-V system can be obtained by minimizing Equation 8 and 11 with respect to y_{v} as follow:

$$\ln \frac{y^{\mathrm{eq}}_{\mathrm{v}}}{1 - y^{\mathrm{eq}}_{\mathrm{v}}} = -\frac{(G_{\mathrm{v}} + y_{\mathrm{Sn}} L_{\mathrm{SnV}} + 2 y_{\mathrm{v}} A \Delta H_{2\mathrm{v}})}{RT} \quad (12)$$

We did not find any information about the changing of the equilibrium concentration of vacancies in relation to the concentration. In the calculation below, it is assumed that the influence of the concentration on the equilibrium fraction of vacancies can be neglected.

5.2. Effect of vacancies on the partition coefficient

The partial free energy of each species must be known in order to analyse the effect of vacancies on the partition of alloying elements between liquid and solid. The partial molar free energy for different species in the solid state can be derived:

$$\bar{G}^{\mathrm{s}}_{\mathrm{Cu}} = G^{0,\mathrm{s}}_{\mathrm{Cu}} + y_{\mathrm{v}} G_{\mathrm{v}} + RT\big(\ln y^{\mathrm{s}}_{\mathrm{Cu}} + y_{\mathrm{v}} \ln y_{\mathrm{v}} + (1 - y_{\mathrm{v}}) \ln(1 - y_{\mathrm{v}})\big) + L_{\mathrm{CuSn}} y^{\mathrm{s}}_{\mathrm{Cu}} \big(1 - y^{\mathrm{s}}_{\mathrm{Cu}}\big) + L_{\mathrm{CuV}} y^{\mathrm{s}}_{\mathrm{Cu}} y_{\mathrm{v}} \quad (13)$$

$$\bar{G}^{\mathrm{s}}_{\mathrm{Sn}} = G^{0,\mathrm{s}}_{\mathrm{Sn}} + y_{\mathrm{v}} G_{\mathrm{v}} + RT\big(\ln y^{\mathrm{s}}_{\mathrm{Sn}} + y_{\mathrm{v}} \ln y_{\mathrm{v}} + (1 - y_{\mathrm{v}}) \ln(1 - y_{\mathrm{v}})\big) + L_{\mathrm{CuSn}} y^{\mathrm{s}}_{\mathrm{Sn}} \big(1 - y^{\mathrm{s}}_{\mathrm{Sn}}\big) + L_{\mathrm{SnV}} y^{\mathrm{s}}_{\mathrm{Sn}} y_{\mathrm{v}} \quad (14)$$

The partial free energy for Cu and Sn in the liquid state is also given:

$$\bar{G}^{\mathrm{l}}_{\mathrm{Cu}} = G^{0,\mathrm{l}}_{\mathrm{cu}} + RT \ln y^{\mathrm{l}}_{\mathrm{Cu}} + L^{\mathrm{l}}_{\mathrm{CuSn}} y^{\mathrm{l}}_{\mathrm{Cu}} \big(1 - y^{\mathrm{l}}_{\mathrm{Cu}}\big) \quad (15)$$

$$\bar{G}^{\mathrm{l}}_{\mathrm{Sn}} = G^{0,\mathrm{l}}_{\mathrm{Sn}} + RT \ln y^{\mathrm{l}}_{\mathrm{Sn}} + L^{\mathrm{l}}_{\mathrm{CuSn}} y^{\mathrm{l}}_{\mathrm{Sn}} \big(1 - y^{\mathrm{l}}_{\mathrm{Sn}}\big), \quad (16)$$

where $G^0 =$ free energy in the standard state of the liquid; $L =$ interaction between Cu and Sn in different states.

The partial free energy of Cu and Sn is equal in the solid and liquid phase at equilibrium, which means:

$$\bar{G}^{\mathrm{l}}_{\mathrm{Cu}} = \bar{G}^{\mathrm{s}}_{\mathrm{Cu}}$$

$$\bar{G}^{\mathrm{l}}_{\mathrm{Sn}} = \bar{G}^{\mathrm{s}}_{\mathrm{Sn}}.$$

Where ΔG represents the resulting change in free energy at a deviation in vacancy concentration from the equilibrium. This fact can be used to calculate the temperature-composition phase diagram of the Cu-Sn system.

Equations 14 and 16 yield the partition coefficient as:

$$k = \frac{y^{s}_{Sn}}{y^{l}_{Sn}} = \exp - \frac{\left(G^{0,l}_{Sn} - G^{0,s}_{Sn}\right) + \left(L^{l}_{CuSn} y^{l}_{Cu}\left(1 - y^{l}_{Cu}\right) - L^{s}_{CuSn} y^{s}_{Cu}\left(1 - y^{s}_{Cu}\right) - L_{SnV} y^{s}_{Sn} y_{v}\right) - y_{v}\Delta G_{v}}{RT} \quad (17)$$

It is interesting to note that the partition coefficient will decrease with an increasing fraction of vacancies.

5.3. Effect of vacancies on the melting point

The free energy of a solid will increase with the fraction of vacancies. From this, the effect of vacancies on the melting point can be obtained.

Following Fredriksson [20], combining Equation 13 with 15 and rewriting the results gives:

$$\Delta T = \Delta T_{Cu} + \frac{RT y^{l}_{Sn}(1-k)}{\Delta H_{tab} + y^{eq}_{v}\Delta H_{v}} \quad (18)$$

The change in melting point for small concentrations of Sn can be calculated using Equation 18. ΔT_{Cu} is the decrease in melting point as a function of the fraction of vacancies when $y_{Sn} = 0$. This has been presented and discussed in detail in the earlier work [19].

$$\Delta T_{Cu} = \frac{RT T_{m}\left(y_{v}\ln\frac{y_{v}}{y^{eq}_{v}} + (1-y_{v})\ln\left(\frac{1-y_{v}}{y^{eq}_{v}}\right)\right)}{\Delta H_{tab}} \quad (19)$$

An increase in the fraction of vacancies increases the free energy of the solid phase. Resulting decrease melting temperature was experimentally observed in Fig. 4.

Combining Equations 17 and 18 can assist to calculate the phase diagram for Cu-Sn system; the results are given in Fig. 7. The solid line represents the equilibrium concentration of vacancies and the dashed lines is obtained for different fraction of vacancies. The calculations show that the solidification temperature decreases with an increase in vacancy concentration.

One can compare the calculated phase diagram for Cu-Sn under equilibrium condition and with a vacancy concentration, which is roughly 50 times the equilibrium values. It was earlier explained [19] that for a pure substance such as copper, the decrease in the solidification temperature is limited to the maximum fraction of vacancies formed; while the maximum vacancy concentration can be obtained from the density difference between solid and liquid.

Fig. 7 also shows that the liquidus temperature for the alloys decreases due to an increase in vacancies and alloying elements. From Equation 18 it can be concluded that the largest undercooling temperature can be achieved when k goes to zero.

5.4. Effect of the vacancies on the latent heat of fusion

The fraction of vacancies also changes the heat of fusion. It was previously shown [18, 19] that the heat of fusion for pure Cu changes by the fraction of vacancies multiplied by the heat of formation of vacancies:

$$\Delta H_{meas} = \Delta H_{tab} - \left(y_{v} - y^{eq}_{v}\right)\Delta H_{v}. \quad (20)$$

In order to calculate the heat of fusion with the trapped concentration of vacancies in Cu-Sn systems, it is necessary to take the interaction between copper and tin atoms, and the effect of the formation of divacancies into account. The change in the energy of formation for a pair of vacancies, when the distance between their centres is comparable to the diameter of a single vacancy should also be analysed. To determine the concentration of divacancies at high temperatures, it is necessary to analyse the formation, migration and binding enthalpies of vacancies determined from non-equilibrium solidification experiments in detail. Unfortunately, values of the formation and binding energies are not well known (look Siegel [17]). In this study and in the absence of such detailed information, it is assumed that the enthalpy of formation of mono-vacancies and divacancies can vary when more vacancies are formed.

Therefore, Equation 20 needs to be modified in order to calculate the change in latent heat with formation and condensation of vacancies in a Cu-Sn system.

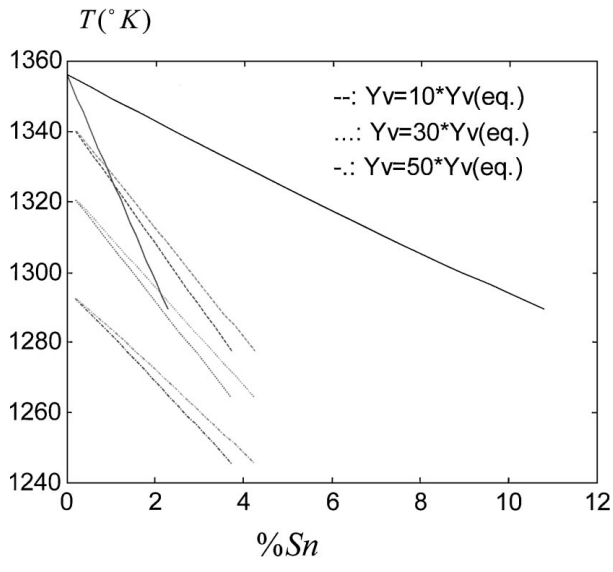

Figure 7 Phase diagram for Cu-Sn system.

$$\Delta H_{\text{meas}} = \Delta H_{\text{tab}} - \left(y_{\text{v}} - y_{\text{v}}^{\text{eq}}\right)\Delta H_{\text{v}} - y_{\text{Cu}} y_{\text{sn}} L_{\text{cuSn}} - y_{\text{v}} y_{\text{v}} A \Delta H_{2\text{v}} \quad (21)$$

The last term on the right hand side describes the formation of divacancies from pre-existing mono-vacancies. The constant A in this relation is 15 according to H. Fredriksson [20]. This value was found by taking the minimum in the free energy of formation of divacancies, as follows:

$$\Delta G_{2\text{v}} = \Delta H_{2\text{v}} - T\Delta S_{2\text{v}} \quad (22)$$

$$S_{2\text{v}} = 2y_{\text{v}} \exp\left(-\frac{\Delta G_{2\text{v}}}{RT}\right) \quad (23)$$

$$\Delta H_{2\text{v}} = A \exp\left(-\frac{\Delta G_{2\text{v}}}{RT}\right) \quad (24)$$

This has been explained in detail elsewhere [20]. The relation for pure copper can also be described as:

$$\Delta H_{\text{meas}} = \Delta H_{\text{tab}} - \left(y_{\text{v}} - y_{\text{v}}^{\text{eq}}\right)\Delta H_{\text{v}} - y_{\text{v}} y_{\text{v}} A \Delta H_{2\text{v}} \quad (25)$$

In this work, it is assumed that the energies of formation of vacancies and divacancies changes with the increasing fraction of vacancies and divacancies. Furthermore, the difference in density between the solid and the liquid is assumed to cause most of the fraction of formed vacancies. These approximations together with Equations 18–25 and data presented in Table III, can be used to calculate solidification undercooling and the latent heat of fusion for solidification.

The results of such calculations together with the experimental measured data for pure copper, Cu-6%Sn and Cu-4% Sn are shown in Fig. 8a–c. The solid lines are calculated on the assumption that no divacancies were formed, and show that the latent heat of fusion reaches zero at high molar fractions of vacancies. The dashed lines represent the latent heat of fusion when the divacancies form.

5.5. Condensation of vacancies

It was previously discussed that a large fraction of vacancies are created during rapid solidification. The number exceeds the equilibrium value. The fraction of vacancies changes during cooling and with the cooling rates; at very high cooling rates, such as in the levitation experiments. an unordered solid state is expected to form with a large supersaturation of vacancies preserved at room temperature. This is due to the fact that there is insufficient time for the vacancies to diffuse and create clusters, to form dislocations or move to grain boundaries.

This will effect the specific heat for the solid, which was shown earlier in Fig. 6. This effect can be analysed using the following relation:

$$C_{\text{p}}^{\text{s}} = C_{\text{p}}^{\text{s},0} + \Delta H_{\text{v}} \frac{\text{d}y_{\text{v}}}{\text{d}T} \quad (26)$$

In this equation, $\text{d}y_{\text{v}}/\text{d}T$ describes the change in the fraction of vacancies or divacancies caused by the decreasing temperature. This term can be replaced by:

$$\frac{\text{d}y_{\text{v}}}{\text{d}T} = \frac{\text{d}y_{\text{v}}}{\text{d}t}\frac{\text{d}t}{\text{d}T} \quad (27)$$

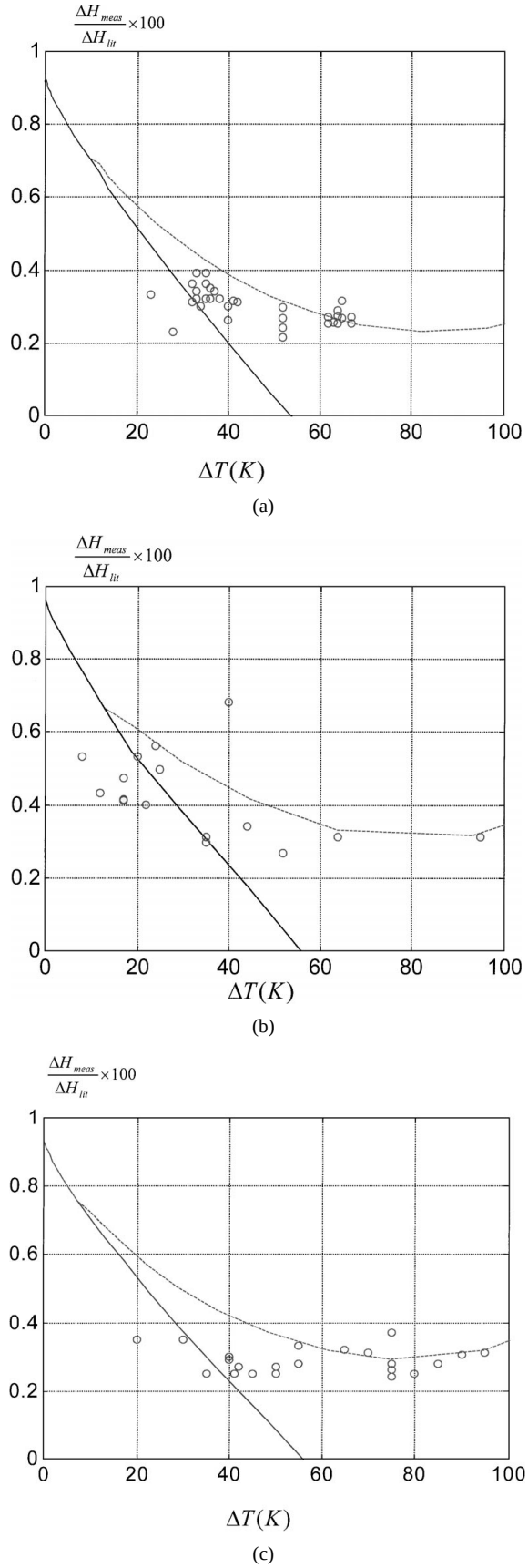

Figure 8 Heat of fusion vs. undercooling temperature for a) Cu, b) Cu-4%Sn and c) Cu-6% Sn.

where dy_v/dt describes the rate of condensation of vacancies or divacancies in the solid phase and dt/dT is the inverse of the cooling rate.

Vacancies are created at the liquid-solid interface at a concentration that corresponds to the liquid–solid density difference. Excess vacancies (those exceeding the equilibrium number) are trapped when they are unable to diffuse back to the rapidly moving interface. The vacancies can also be expected to form larger clusters or dislocations or to move to the grain boundaries at lower cooling rates. This means that vacancies will be condensed gradually at dislocations and grain boundaries. It has earlier been mentioned [9] that the diffusion process of vacancies can be described by a squared sin-function as follow:

$$y_v^C = \left(y_v^{max} - y_v^{eq}\right) - \left(y_v^{max} - y_v^{eq}\right)\frac{4}{\pi} \times \exp\left(-\frac{4\pi^2 Dt}{l^2}\right)\sin\frac{2\pi S}{l} \quad (28)$$

where y_v^C: molar fraction of condensed vacanies; y_v^{max}: maximum molar fraction of frozen in vacancies; y_v^{eq}: equilibrium molar fraction of vacancies; l: wavelength; S: distance.

The total fraction of condensed vacancies can be calculated by integrating this expression over the distance between vacancy sinks

$$\frac{2\lambda A}{V_m}\Delta y_v = \int_0^{2\lambda} f(y_v)dx\frac{A}{V_m}, \quad (29)$$

where $l = 4\lambda$; λ: the distance between two sinks for vacancies; A: surface area; V_m: molar volume.

Which gives:

$$\Delta y_v = \left(y_v^{max} - y_v^{eq}\right)\left[1 - \frac{8}{\pi^2}\exp\left(-\frac{\pi^2 Dt}{4\lambda^2}\right)\right], \quad (30)$$

Equation 30 describes the molar fraction of condensed vacancies. The change in C_P with the cooling rate can be calculated by derivating Equation 30 and combining it with Equations 26 and 27, one gets:

$$C_P^s = C_P^{s,o} + \Delta H_v\left(y_v^{max} - y_v^{eq}\right)\frac{2D}{\lambda^2}\exp\left(-\frac{\pi^2 Dt}{4\lambda^2}\right)\frac{dt}{dT} \quad (31)$$

The results of calculation of C_P for different cooling rates as a function of time are shown in Fig. 9a and b. The figure shows that at high cooling rates the second term in Equation 31 has a very little effect on the C_P due to the very low value on the inverse cooling rate term. No vacancies will have time to condense.At lower cooling rates the possibilities for condensation of vacancies increases and one will get higher value on the C_P. At very low cooling rates it can be expected that all the vacancies will be condensed before the solidification process has finished. In such a case the C_P value will agin correspond to the tabulated value.

It should be pointed out that the calculations at low cooling rates are very sensitive to the selection of the

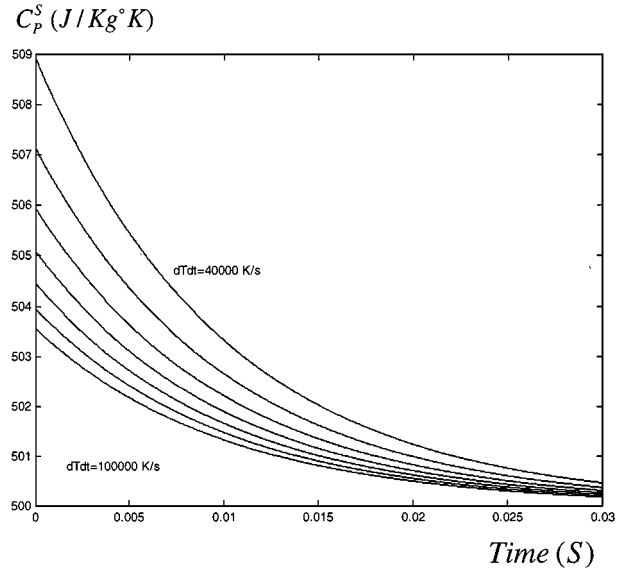

(a)

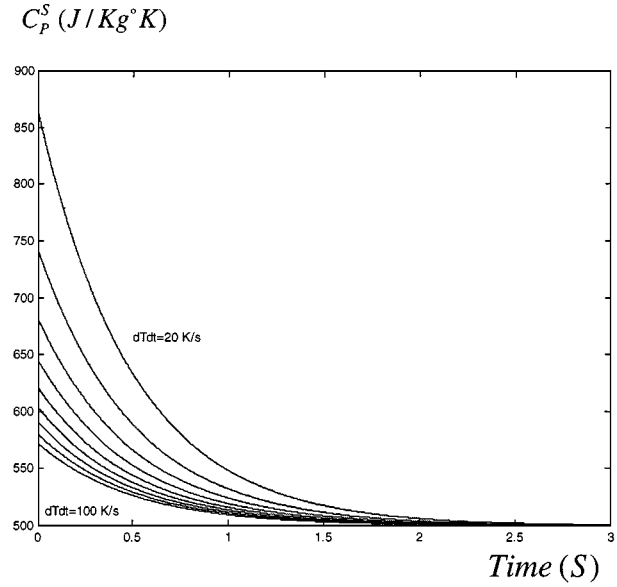

(b)

Figure 9 Specific heat vs. condensation times at different cooling rates for a) levitation and b) mirror furnace experiments.

distance between two sinks of vacancies due to a second power effect of λ in Equation 31. This sensitivity is illustrated in a series of calculations shown in Fig. 10. Here, the cooling rate is assumed to be equal 50 K s^{-1} and the λ value has been varied from 4 to 8 μm. The results indicate that with a shorter value of the λ, one gets a higher value of C_P which rapidly drop down to the tabulated value. Further, at a longer distance between two sinks of vacancies, the condensation of vacancies will take place more slowly and the effects on C_P will not be large, specially at the end of the solidification process, instead, it will preserve for a longer time. However, it seems reasonable to choose a value of the distance between the secondary dendrite arms, which is normally related to the cooling rate.

This phenomenon for Cu-Sn systems at very low cooling rates will be discussed in a later paper.

It should finally be mentioned that the presented calculations were performed only for the formation of

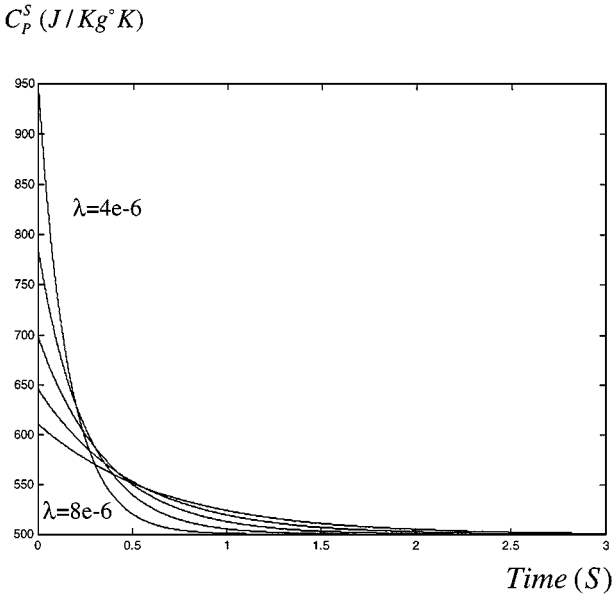

Figure 10 Specific heat vs. condensation times for different λ.

vacancies during rapid solidification. It is worth noting that the introduction of such a large number of vacancies in a lattice, not only causes a change in the total volume of the metal but also acts as a source for the creation of other types of lattice defects such as dislocations and stacking faults. However, more experimental data is needed in order to verify the way that the various types of point defects move and interact with each other. It is necessary to measure continuously certain property of the pure metal or alloy which directly depend on the formation, migration and annihilation of vacancies, interstitials and complexes of these defects with other impurities.

6. Concluding remark

The solidification behaviour of Cu-Sn alloys during a rapid solidification process has been studied. The calculation of specific heat capacity and latent heat of fusion were integrated to a FEM solidification program. The following main conclusion can be drawn:

a) The undercooling temperature increases with increasing cooling rate.

b) The heat of fusion decreases as a function of increasing cooling rate.

c) Calculated values for ΔH are much lower than tabulated ones.

d) Calculated values for the specific heat in the solid zone for mirror furnace experiments are much higher than tabulated ones. This can be explained by the condensation of vacancies.

e) The partition coefficient will decrease with an increasing fraction of vacancies.

f) The liquidus temperature in the phase diagram for Cu-Sn system decreases with an increase in vacancy concentration.

g) The excess fraction of vacancies, penetrated into the lattice, decrease the latent heat of fusion.

h) The effect from formation of vacancies on the solidification behaviour should be reconsidered.

Acknowledgements

This work is partly supported by Outokumpu Partner AB and partly by NUTEK. J.M is grateful for the scholarship from the Iranian Research Organisation for Science and Technology, I.R.O.S.T.

References

1. W. A. TILLER, *J. Appl. Phys.* **29** (1958) 611.
2. R. S. WAGNER, *ibid.* **29** (1958) 1769.
3. P. E. DOHERTY and R. S. DAVIS, *Acta Met.* **7** (1959) 118.
4. G. F. BOLLING and D. FAINSTEIN, *The Philosophical Magazine* **25** (1978) 45.
5. T. GORECKI, *Ber. Bunsenges. Phys. Chem.* **87** (1983) 801.
6. L. BATTEZATI and M. BARICO, *J. Less-Common Met.* **145** (1988) 31.
7. L. LIU and Y. DONG, *J. Mater. Sci. Technol* **10** (1994) 232.
8. A. MUNITZ. S. P. ELDER-RANDALL and R. ABBASCHIAN, *Metall. Trans. A* **23A** (1992) 1817.
9. M. H. SABZEVAR and H. FREDRIKSSON, Thesis, Stockholm, 1994.
10. N. EL. MAHALLAWY, M. TAHA and H. FREDRIKSSON, *Mater. Sci. Eng.* **A179**/**A180** (1994) 587.
11. R. BENEDEK, *J. Phys. F: Met. phys.* **17** (1987) 569.
12. U. KÖSTER, *Key Eng. Mate.* **81-83** (1993) 647.
13. S. M. KIM, *Physical Review* **30** (1984) 30.
14. M. J. GILLAN, *J. Phys.: Condens. Matter* **1** (1989) 689.
15. H. M. POLATOGLOU, M. METHFESSEL and M. SCHEFFLER, *Phys. Rev. B* **48** (1993) 1877.
16. S. J. ZINKLE, L. E. SEITZMAN and W. G. WOLFER, *Philosophical Magazine A* **55**(1) (1987) 111.
17. R. W. SIEGEL, *J. Nuclear Mater* **69-70** (1978) 117.
18. S. BERG, J. DAHLSTRÖM and H. FREDRIKSSON, *ISIJ int.* **35** (1995) 876.
19. J. MAHMOUDI and H. FREDRIKSSON, *Mater. Sci. Eng.* **A226-228** (1997) 22.
20. H. FREDRIKSSON and T. EMI, *Mater. Trans., JIM* **39** (1998).
21. J. LIU, N. JACOBSSON and H. FREDRIKSSON, Thesis, Stockholm, 1992.
22. C. LOCKOWANDT, K. LÖTH and A. JARFORS, in VIII Eur. Symp. Mater. Fluid Sci. 12–16 April, Brussels, Belgium, 1992.
23. B. ROBERG, *Scand. J.Met.* **12** (1983) 13.
24. Femgv Ver 4.0, Femsys Limited, 1996.
25. C. J. SMITHELLS, "Metals Reference Book" (London, 1976).
26. Y. S. TOULOUKIAN, TPRC Data Series, 1970.
27. W. R. BITLER and P. MOLL, Final Report INCRA Proj. No. 245, 1981.
28. J. N. MUNDY, *Phys. stat. sol* (B) **144** (1987) 233.
29. R. D. PEHLKE, A. JEYARAJAN, H. WADA, NSF/MEA-82028, NTIS, Michigan Univ., 1982.
30. B. SUNDMAN, "Thermoclac" (Royal Inst.of Tech., Stockholm, 1993).
31. A. SEEGER, *Crystal Lattice Defect* **4** (1973) 221.
32. N. H. MARCH and J. S. ROUSSAU, *ibid.* **2** (1971) 1817.
33. R. W. CHAN and HASSEN, *Phys. Metall.* **2** (1996) 1630.
34. L. KORNBELIT, *Phys. Stat., Sol.* (B) **115** (1983), 485.

Received 27 July 1998
and accepted 30 September 1999